Science Translational Medicine
AAAS

In Vivo–Directed Evolution of a New Adeno-Associated Virus for Therapeutic Outer Retinal Gene Delivery from the Vitreous

Deniz Dalkara *et al.*

Sci Transl Med **5**, 189ra76 (2013);
DOI: 10.1126/scitranslmed.3005708

Editor's Summary

New Eye Pod

Gene therapy mediated by adeno-associated virus (AAV) vectors has been clinically successful for the treatment of certain inherited diseases of the retina —the light-sensitive structure at the back of the eye that houses the photoreceptor cells (rods and cones). These degenerative disorders arise from mutated genes that either fail to express an essential protein or express harmful proteins that drive structural breakdown, cell death, and, ultimately, blindness. Current gene therapy regimens require damaging injections of gene-carrying vectors into the space between the rod and cone photoreceptors and the retinal pigment epithelium. By this route, the genetic material is delivered to only part of the retina. Now, Dalkara *et al*. show that delivery of a new vector into the eye's easily accessible vitreous humour transduces the entire retina and rescues degenerative eye disease phenotypes.

The authors used in vivo–directed evolution to fashion an AAV vector that delivers wild-type versions of defective genes throughout the retina after noninjurious injection into the eye's easily accessible vitreous humour — the gel-like liquid between the lens and the retina. The newly engineered gene therapy systems rescued disease phenotypes in two mouse models of inherited eye diseases (X-linked retinoschisis and Leber's congenital amaurosis) and transduced photoreceptor cells in nonhuman primates when delivered via the vitreous. Development of these next-generation therapeutic "eye pods" suggests that gene therapy vectors can be designed to penetrate dense tissues, which currently constitute barriers to gene delivery.

Science Translational Medicine (print ISSN 1946-6234; online ISSN 1946-6242) is published weekly, except the last week in December, by the American Association for the Advancement of Science, 1200 New York Avenue NW, Washington, DC 20005.

BLINDNESS

In Vivo–Directed Evolution of a New Adeno-Associated Virus for Therapeutic Outer Retinal Gene Delivery from the Vitreous

Deniz Dalkara,[1]* Leah C. Byrne,[1]* Ryan R. Klimczak,[2] Meike Visel,[2] Lu Yin,[3] William H. Merigan,[3] John G. Flannery,[1,2†] David V. Schaffer[1,2,4†]

Inherited retinal degenerative diseases are a clinically promising focus of adeno-associated virus (AAV)–mediated gene therapy. These diseases arise from pathogenic mutations in mRNA transcripts expressed in the eye's photoreceptor cells or retinal pigment epithelium (RPE), leading to cell death and structural deterioration. Because current gene delivery methods require an injurious subretinal injection to reach the photoreceptors or RPE and transduce just a fraction of the retina, they are suitable only for the treatment of rare degenerative diseases in which retinal structures remain intact. To address the need for broadly applicable gene delivery approaches, we implemented in vivo–directed evolution to engineer AAV variants that deliver the gene cargo to the outer retina after injection into the eye's easily accessible vitreous humor. This approach has general implications for situations in which dense tissue penetration poses a barrier for gene delivery. A resulting AAV variant mediated widespread delivery to the outer retina and rescued the disease phenotypes of X-linked retinoschisis and Leber's congenital amaurosis in corresponding mouse models. Furthermore, it enabled transduction of primate photoreceptors from the vitreous, expanding its therapeutic promise.

INTRODUCTION

Inherited forms of retinal degeneration, which afflict 1 in 3000 people worldwide, arise primarily from mutations in cells of the eye's outermost retinal layer (Fig. 1). These include photoreceptor cells—light-detecting neurons in the retina of vertebrate eyes—or cells of the retinal pigment epithelium (RPE)—a layer of pigmented cells that lies just outside of and supports the photoreceptors. The outer retina is, therefore, the primary target for ocular gene therapies (*1*), which deliver a wild-type copy of the mutated gene to the appropriate cells (transduction) typically by using an adeno-associated virus (AAV) vector.

Current gene delivery vehicles require administration into the subretinal space between the RPE and the photoreceptors to transduce these neurons. To achieve delivery of the vector, a needle must penetrate the retina and, in doing so, detaches the photoreceptor cell layer from the RPE (*2*, *3*). Three recent clinical trials for the retinal disease type 2 Leber's congenital amaurosis (LCA2) used subretinal injections to deliver AAV that carried the retinal isomerase–encoding gene *RPE65* to the RPE; the trial protocol benefited from the atypical pathology of LCA2, which exhibits a loss of photosensitive function without significant structural disruption of retinal layers for many years (*4*–*8*). In contrast, most retinal degenerative diseases (including retinitis pigmentosa and macular degeneration, which account for half of all retinal degeneration cases) are characterized by the progressive loss of photoreceptor cells and increasingly fragile retinal architecture across the entire retina (*9*, *10*). In such disease states, subretinal surgery can induce mechanical damage, reactive gliosis, and loss of function (*8*, *11*). These procedural effects have even been documented in one LCA2 trial, as patients receiving a subretinal injection under the foveal region lost retinal thickness and visual acuity; these results led investigators to conclude that LCA gene therapy is efficacious in the extrafoveal retina but offers no benefit and some risk in treating the fovea (*12*).

X-linked retinoschisis (XLRS) is a retinal degenerative disease caused by mutations in transcripts expressed in the outer retina and is amenable to clinical gene therapy. XLRS mutations reside in the gene encoding the retinoschisin protein and lead to particularly severe structural abnormalities and compromised vision. This protein, ordinarily secreted from photoreceptors, is required for maintenance of normal retinal organization including the photoreceptor–bipolar cell synapse (*13*). Gene therapy studies in the XLRS knockout mice, null for retinoschisin (*Rs1h*), illustrate the challenges for XLRS gene replacement therapy in patients. Intravitreal and subretinal approaches have been used to deliver AAV carrying a functional copy of the *Rs1h* gene in this model (*14*). However, photoreceptors were efficiently transduced only with the subretinal injections, which both limited the region of therapeutic effect and caused surgical disruption at the injection site (*15*, *16*).

How well retinas of patients with retinal degenerative disease can tolerate subretinal surgery will depend on the nature of the mutation and the stage of the retinal degeneration at which the surgery is performed. As an additional concern, because outer retinal defects are expressed across the tissue, an effective treatment should be pan-retinal or reach cells along the entire width of the retina; subretinal injections transduce only cells that contact the local "bleb" of injected fluid. Therefore, a new delivery technology is needed for gene transfer to deeper layers of the retina. Such a technique could have broader implications for treating human diseases that involve cells within structurally complex tissues that are inaccessible to AAV as a result of physical (for example, diffusion and membranes) and cellular barriers (for example, endothelial cells).

[1]Helen Wills Neuroscience Institute, University of California, Berkeley, CA 94720–1462, USA. [2]Department of Molecular and Cellular Biology, University of California, Berkeley, CA 94720–1462, USA. [3]Flaum Eye Institute and Center for Visual Science, University of Rochester, Rochester, NY 14642, USA. [4]Department of Chemical and Biomolecular Engineering, University of California, Berkeley, CA 94720–1462, USA.
*These authors contributed equally to this work.
†Corresponding author. E-mail: schaffer@berkeley.edu (D.V.S.); flannery@berkeley.edu (J.G.F.)

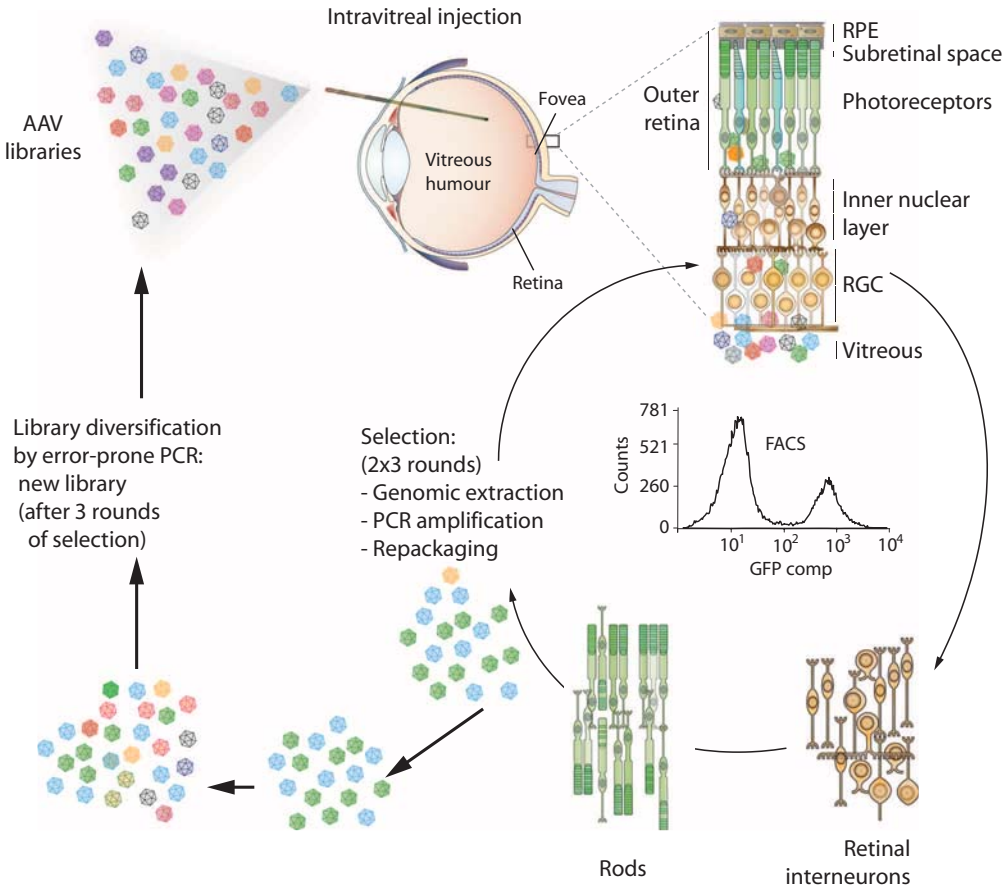

Fig. 1. Schematic of in vivo–directed evolution process used to generate viral variants. Three libraries were created: an error-prone AAV2 Y444F library, an AAV shuffled library, and a random 7mer insertion library. Each library had a diversity of 10^7, and they were mixed in equal parts and injected intravitreally into adult transgenic rho-GFP mice eyes. One week after injection, eyes were enucleated and retinas were dissociated using a mild papain protease treatment, followed by FACS isolation of photoreceptors (representative FACS plot). Viral *cap* genes from the isolated cells (representing the AAV variants from the library that successfully transduced photoreceptors) were then PCR-amplified from genomic extractions for cloning and repackaging. One round of evolution consisted of initial library diversification followed by three selection steps. RGCs, retinal ganglion cells; RPE, retinal pigment epithelium.

To endow AAV with the ability to overcome such complex tissue barriers, we developed an in vivo–directed evolution strategy that enabled us to iteratively enrich for AAV variants capable of reaching the outer retina from the vitreous. Here, we describe an evolved AAV variant (7m8) that mediated highly efficient delivery to all retinal layers in mice and nonhuman primates. 7m8 also mediated therapeutic gene delivery to photoreceptors in two mouse models of retinal disease, enabling non-invasive, long-term histological and functional rescue of disease phenotypes across the entire retina. These findings have important and immediately clinically relevant implications for the development of gene therapies for LCA2, retinoschisis, and other retinal diseases requiring robust, pan-retinal gene expression without retinal detachment.

RESULTS

Naturally occurring AAV serotypes cannot transduce photoreceptors from the vitreous side of the retina (*17*, *18*) because the inner limiting membrane (ILM) and intervening neuronal and glial cells and processes of the inner retina (Fig. 1) form a formidable diffusive barrier with abundant binding sites for AAV particles that is several hundred micrometers thick in rodents and primates (*19*, *20*). Rational mutagenesis of surface-exposed tyrosine residues, which allows AAV particles to avoid intracellular ubiquitination and degradation, increases intravitreal photoreceptor gene delivery through improved intracellular nuclear trafficking and thereby indicates that AAV2 has the partial ability to infect photoreceptors from the vitreous (*21*, *22*). However, decreasing intracellular ubiquitination is secondary to the substantial physical barriers a vector encounters during infection, which in this case may include viral sequestration, poor diffusion in the ILM, extracellular spaces, and intervening cell layers, or both.

Library screening converges on one dominant variant

To develop an AAV capable of outer retinal gene delivery upon intravitreal injection, we designed an in vivo–directed evolution approach (Fig. 1). Three AAV libraries, each with a diversity of 10^7, were used: an AAV2 capsid protein (*cap*)–encoding library with a random seven–amino acid sequence inserted into loop 4 (within the heparin-binding domain) of the capsid (*23*, *24*); a library that encoded a tyrosine mutant version of the AAV2 genome (*25*) subjected to random mutagenesis (AAV2 Y444F EP); and a chimeric capsid–encoding library generated by shuffling AAV1, 2, 4, 5, 6, 8, and 9 (*26*). The libraries were combined and injected intravitreally into the eyes of transgenic mice that expressed a rhodopsin–green fluorescent protein (GFP) fusion specifically in their rod photoreceptors (*27*). Fluorescence-activated cell sorting (FACS) was optimized to isolate pure, GFP-positive photoreceptors from harvested retinas 1 week after library injection. Successful AAV *cap* variants were then recovered from these neurons by polymerase chain reaction (PCR), and virus was again packaged. Two more such selection steps were conducted, followed by error-prone PCR to introduce further diversity into the library, and three additional in vivo selection steps were carried out.

After this extended evolution process, 48 variant *cap* genes were sequenced (Fig. 2A). Notably, 46 of these clones originated from the AAV2 seven–amino acid peptide (7mer) insertion library, with 31 containing the same seven–amino acid motif (LGETTRP). The next most prominent variant (5 of 46) contained a similar motif (NETITRP) with

A

Clone	Percentage
AAV2 588~ LALGETTRP	67
AAV2 588~ LANETITRP	10
AAV2 588~ LAKAGQANN	6
AAV2 588~ LAKDPKTTN	4

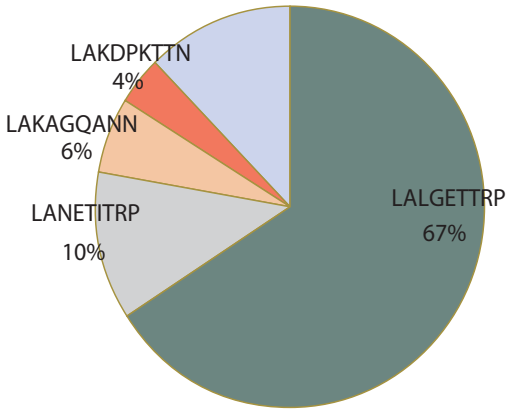

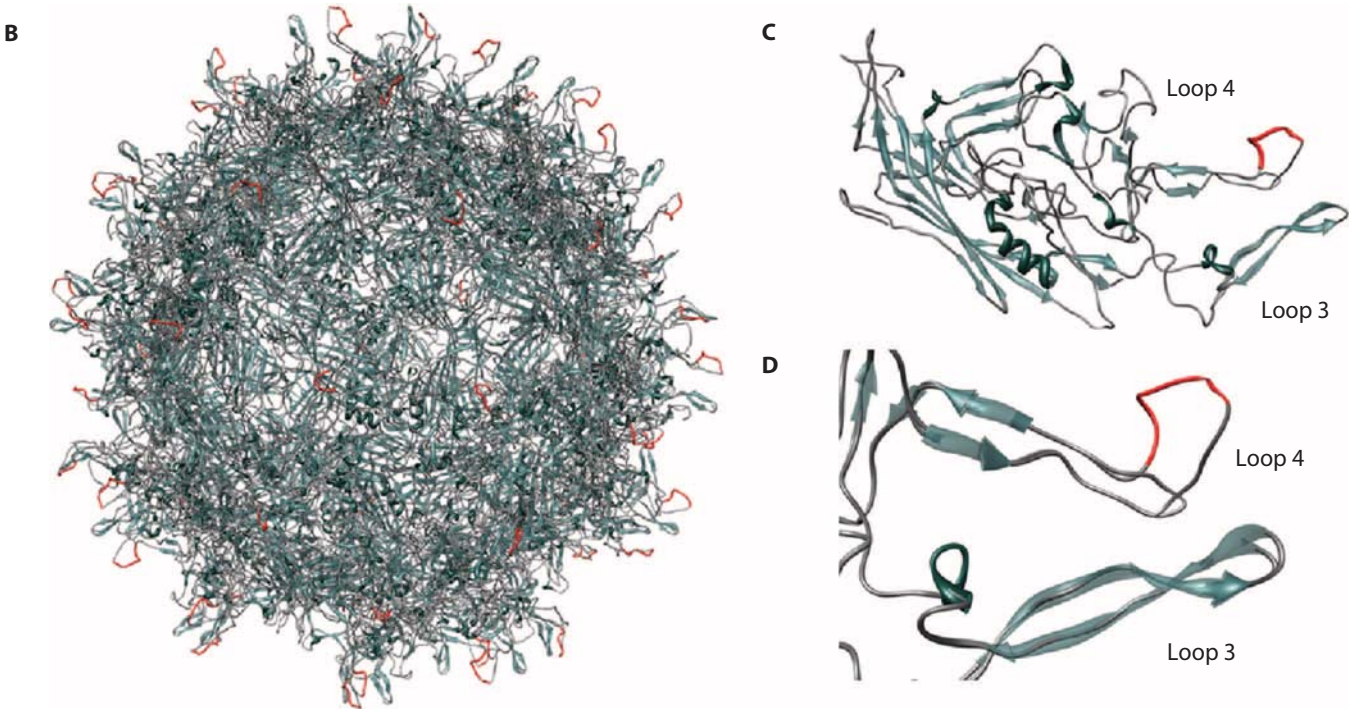

Fig. 2. Characterization of evolved variants and structural modeling of 7m8. (**A**) Sequencing of evolved variants revealed a high degree of convergence in the selected viral pools. All but two sampled variants originated from the AAV2 seven–amino acid library, and 67% of all clones (32 of 48) contained the same 7mer motif (LGETTRP). The remainder, not included in the table, were represented only once within the population. (**B** to **D**) Molecular model of AAV2 containing the insertion LALGETTRP (shown in orange) after amino acid 587. The interactions between the inserted loop and the other surface loops of the capsid likely play a role in the novel properties of the virus.

a positively charged arginine residue in between a polar threonine and a nonpolar proline residue (TRP). This represents a convergence from ~10^7 input variants down to a single dominant consensus sequence. In addition, 34 of the 46 clones coming from the 7mer library harbored a V708I mutation. We focused on one of these prominent clones, 7m8, for in-depth characterization.

We modeled the major capsid protein of 7m8, that is, AAV2~^{588}LALGETTRP, superimposed on its parent AAV2 (Fig. 2B). The ^{588}LALGETTRP insertion disrupted basic arginine residues in loop 4 implicated in AAV2 binding to its primary receptor, heparan sulfate proteoglycan (HSPG) (*28*) (Fig. 2, C and D). In addition, the peptide's location in loop 4 and proximity to loop 3 (also involved in receptor binding) place it in a position to further alter viral tropism. 7m8 was used to package recombinant virus carrying the gene encoding GFP (7m8-GFP), and its glycan dependencies (fig. S1A) were analyzed in vitro. 7m8 infection was still HSPG-dependent (*28*), although its heparin affinity was lower compared to AAV2 (fig. S1B). In addition, like AAV2, 7m8 showed no sialic acid dependence; however, it was >10- to 100-fold more infectious than AAV2 in Chinese hamster ovary (CHO) cell lines.

In vivo characterization shows pan-retinal reporter gene expression with 7m8

To assess the capacity of 7m8 to mediate gene delivery to the outer retina, we injected 7m8-GFP intravitreally into adult wild-type mice, which resulted in strong pan-retinal GFP expression that was readily visualized via fundus imaging (Fig. 3A). In addition, 6 weeks after injection, retinal flat mounts, imaged with the outer nuclear layer facing upwards, showed marked GFP expression in photoreceptors across the retina (Fig. 3B and fig. S2), and a montage of transverse cryosections further demonstrated pan-retinal expression (Fig. 3C). Higher-magnification imaging revealed that although AAV2-mediated expression was limited to RGCs and some Müller glia (Fig. 3D), 7m8 led to marked expression, not only within RGCs and Müller cells but also in amacrine cells, bipolar cells, rods, cones, and RPE (Fig. 3, E and F).

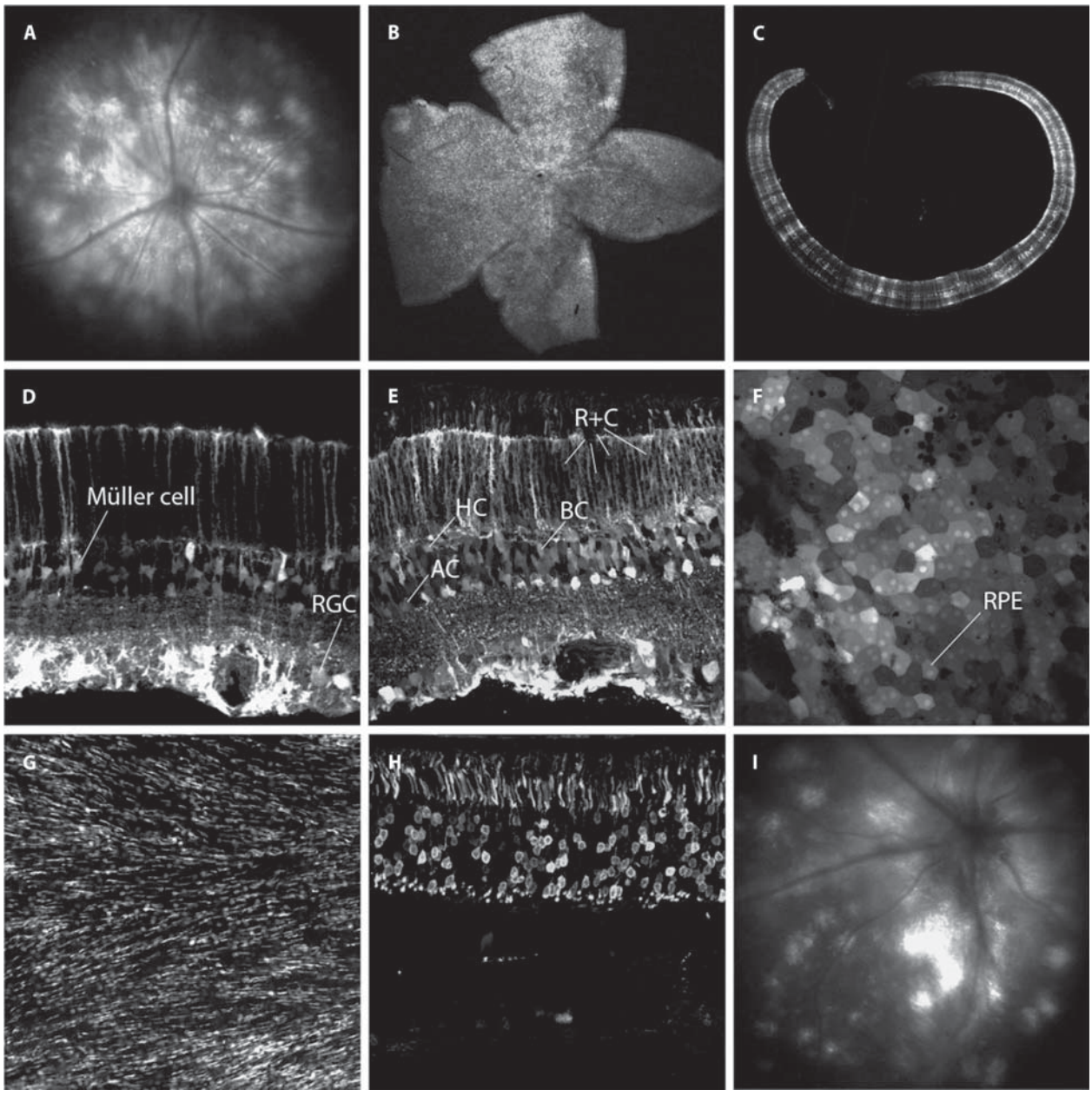

Fig. 3. Pan-retinal transgene expression in photoreceptor cells using 7m8. (**A**) Fundus image of a wild-type (WT) mouse retina 3 weeks after injection with 7m8-scCAG-GFP, showing pan-retinal gene expression. (**B**) A retinal flat mount oriented with the outer nuclear layer facing upwards shows GFP expression in photoreceptor cell bodies and outer segments across the retina. (**C**) Montage of confocal images showing unamplified pan-retinal GFP expression in a WT retina after injection with 7m8-scCAG-GFP. (**D** and **E**) Confocal microscopy of transverse retinal sections 6 weeks after intravitreal injection of 1 μl of AAV2 [1×10^{12} viral genomes (vg)/ml] (D) or 7m8 (E) in adult WT mice shows greater transduction of the outer retina in eyes injected with 7m8 compared to the parental serotype. (**F**) GFP expression in flat mounted RPE after injection of 7m8-scCAG-GFP. (**G** to **I**) GFP expression restricted to photoreceptors using a rhodopsin promoter. (G) Flat mount retina, (H) cross section, and (I) fundus images showing in vivo expression of 7m8-rho-GFP.

These results establish that positive selection for localization to photoreceptors resulted in substantially enhanced transduction of this important cell type, although not surprisingly, it did not select against transduction of other neurons or RPE. Because 7m8 is capable of transducing cells far away from the injection site, we assessed whether this variant remained restricted to the retina by examining brain sections of mice after intravitreal 7m8-GFP delivery. The optic nerve from the injected eyes showed high levels of GFP expression detectable through the optic tract, with the GFP-positive axons of RGCs traveling to the suprachiasmatic nuclei and lateral geniculate nuclei; however, there were no GFP-positive cell bodies (fig. S3) in either brain region. Furthermore, 7m8 carrying a rod-specific rhodopsin promoter (7m8-rho-GFP), rather than the ubiquitous CAG promoter, successfully restricted expression to photoreceptors (Fig. 3, H and I). These results indicate that we created an AAV variant able to transduce all retinal cell types after intravitreal administration and that coupling this capsid with a promoter of interest can target expression to a specific cell type.

We next compared the transduction properties of 7m8 to the AAV vector that reportedly provides the best photoreceptor transduction profile when injected into the vitreous, a quadruple tyrosine mutant AAV2 (AAV2-4YF) (*21*, *22*). Particles (10^{11}) of both 7m8-rho-GFP and AAV2-4YF-rho-GFP were injected into the vitreous cavity of four wild-type mice eyes. Reverse transcription PCR (RT-PCR) was conducted to quantify GFP mRNA levels, and 7m8 showed a fivefold increase over AAV2-4YF in the murine retina (fig. S4).

Last, we investigated immune reactions to the 7m8 capsid upon vector readministration. Intravitreal administration of either AAV2 or AAV5 vectors has been reported to generate a humoral immune response against the viral capsid that blocks vector expression upon subsequent readministration into the partner eye (*29*, *30*). We investigated whether such immune responses to 7m8 were similar to these previously reported findings and did indeed find that after injection of 7m8-GFP in one mouse eye, later injection of 7m8-GFP into the contralateral eye did not lead to GFP expression. Cryosections of these eyes showed the presence of a few activated microglial and macrophage cells in the second eye but no structural damage in either retina (fig. S5).

7m8-RS1 improves structure and rescues function in the *Rs1h*$^{-/-}$ mouse

To evaluate the potential of the 7m8 vector for photoreceptor gene therapy, we used the retinoschisis knockout (*Rs1h*$^{-/-}$) mouse (*13*), which has difficulty tolerating subretinal injections (fig. S6). After injection at P15, early in the development of the *Rs1h*$^{-/-}$ pathology when the retina is largely intact, 7m8-rho-GFP strongly and pan-retinally transduced photoreceptors (fig. S7J). In contrast, AAV2-rho-GFP and AAV8-rho-GFP—which was previously reported to improve the RS1 phenotype when injected 6 to 9 weeks after birth, closer to the peak of cavity formation (*31*)—led to little GFP expression in photoreceptors when administered at P15 (fig. S7).

Intravitreal administration of 7m8-rho-RS1 led to high-level, pan-retinal RS1 expression in photoreceptors and throughout all other retinal layers (Fig. 4, A and B), comparable to wild-type levels of this secreted protein (Fig. 4C). Furthermore, imaging of the photoreceptor–bipolar cell synapse showed that 7m8-rho-RS1 treatment improved synaptic organization (fig. S7, K and L).

The structural improvement observed by immunohistochemistry was corroborated by high-resolution spectral domain optical coherence tomography (SD-OCT) imaging (Fig. 4, D to I). Four months after intravitreal injection of 7m8-rho-GFP into the *Rs1h*$^{-/-}$ mice, retinas were marked by large and pervasive cavities (Fig. 4, D and G). In stark contrast, 7m8-rho-RS1–treated retinas had few cavities, which were barely visible in fundus images (Fig. 4E) and cross sections (Fig. 4H). Also, treated retinas were only slightly thinner than wild-type retinas of the same age (Fig. 4, F and I). By comparison, no structural improvements were observed in retinas treated with AAV2-rho-RS1 or AAV8-rho-RS1 4 months after treatment (fig. S7).

Electroretinography (ERG), which reports retinal function in response to a flash of light, was conducted to analyze rescue of the hallmark functional deficits of retinoschisis. Specifically, the *Rs1h*$^{-/-}$ mouse progressively loses amplitude in the ERG b-wave, which arises from the inner retina, and displays relative preservation of the a-wave, which originates from photoreceptors (*32*).

A time course analysis over 4 months showed that ERG b-waves in 7m8-rho-GFP–injected eyes steadily decreased by 27% to 165.9 ± 17.5 μV, whereas the amplitude in 7m8-rho-RS1–treated eyes was preserved at a significantly higher level of 333.4 ± 15.7 μV (Fig. 4J; $P < 0.0005$, 7m8-rho-GFP versus 7m8-rho-RS1 4 months after injection, two-tailed paired Student's *t* test). In contrast, ERG b-wave amplitudes recorded from eyes injected with AAV2-rho-RS1, AAV8-rho-RS1, or AAV2-rho-GFP were undistinguishable from untreated eyes. In addition, the amplitude of ERGs recorded from 7m8-rho-RS1–treated mice 4 months after injection revealed improvement of the b-wave over a range of stimulus levels under both scotopic (dark-adapted, upper traces) and photopic (light-adapted, lower traces) conditions (Fig. 4K). Furthermore, representative scotopic ERG recordings from 7m8-rho-RS1– and 7m8-rho-GFP–treated eyes at 4 months with the highest stimulus intensity illustrated restoration of ERG amplitude and waveform (Fig. 4L). These results indicate that intravitreal administration of 7m8-rho-RS1 led to substantial and stable improvements of rod and cone photoreceptor-mediated visual function, as well as synaptic transmission over a wide range of lighting intensities.

7m8-RPE65 expression rescues the rd12 phenotype

To generalize the potential of the 7m8 vector for outer retinal gene therapy to another important disease model, we investigated gene replacement therapy in the *rd12* mouse model of LCA, which differs from the retinoschisin model in several key ways. First, in contrast to *Rs1h*$^{-/-}$ mice, *rd12* retinas remain structurally intact until 3 months after birth. In addition, because the *rd12* phenotype results from mutations in the gene encoding RPE-specific protein RPE65, rescue in this model requires transduction of the RPE, which lies beyond the photoreceptor layer and is thus an even more distant and challenging target to infect from the vitreous.

We analyzed the ability of 7m8 to deliver a wild-type copy of the *RPE65* gene in this animal model by administering 7m8-RPE65 into one eye and injecting 7m8-GFP into the contralateral, control eye. Labeling of RPE65 protein in RPE flat mounts (Fig. 5A) revealed expression of the protein in 7m8-RPE65–injected eyes, whereas 7m8-GFP– and AAV2-RPE65–injected eyes lacked any labeling, similar to untreated eyes. RT-PCR (Fig. 5B) revealed that eyes injected with 7m8-RPE65 had increased amounts of RPE65 mRNA, whereas 7m8-GFP–injected eyes expressed amounts of RPE65-encoding mRNA similar to those of untreated eyes.

We assessed functional recovery in *rd12* retinas by electroretinographic analysis of the full-field scotopic b-wave measured 35 days after vector injection ($n = 7$). 7m8-CAG-RPE65 treatment led to a

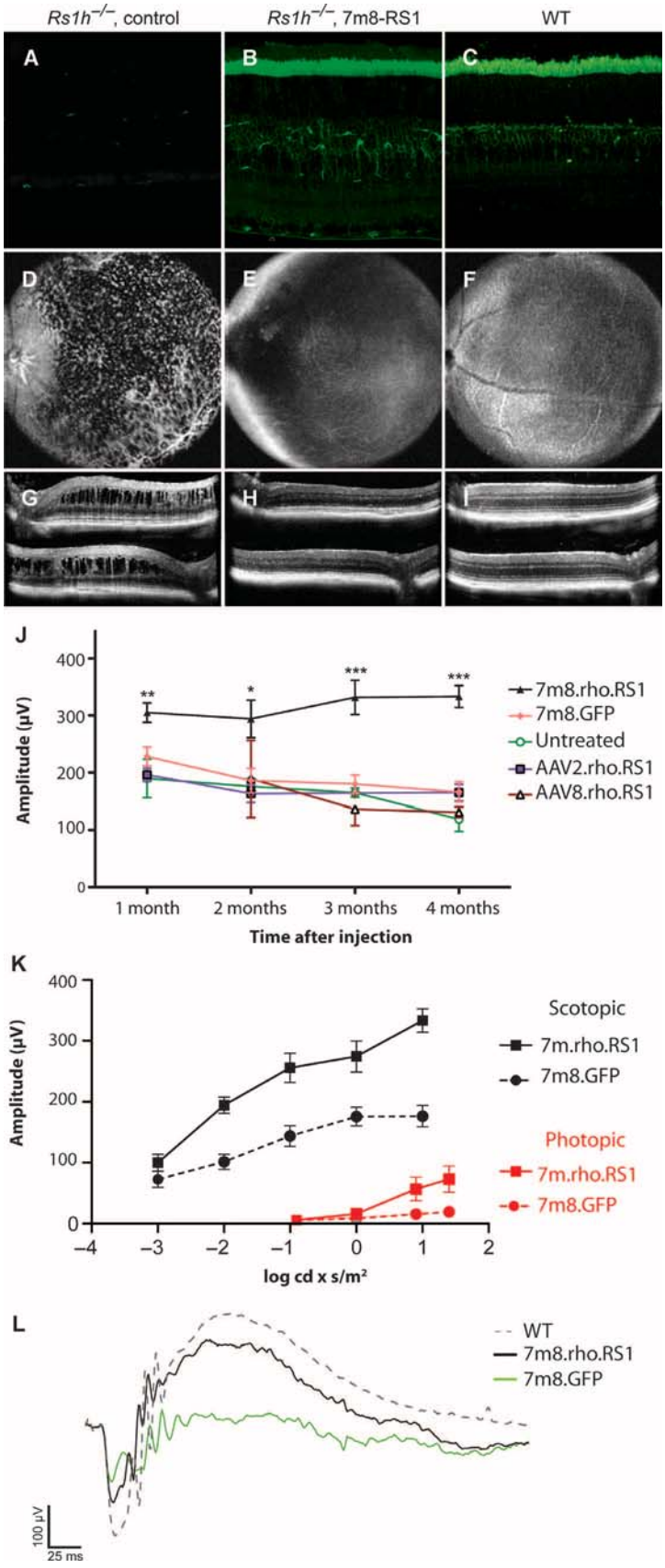

Fig. 4. Structural and functional improvements in the *Rs1h*$^{-/-}$ mouse retina after 7m8-mediated RS1 gene transfer. (**A**) RS1 immunostaining in control *Rs1h*$^{-/-}$ eyes shows absence of the protein. (**B**) Staining of 7m8-rho-RS1–injected eyes shows strong RS1 expression in photoreceptor inner segments, as well as in the outer plexiform layer, inner plexiform layer, and inner nuclear layer. (**C**) Expression of RS1 in a WT eye. (**D** to **F**) Representative high-resolution SD-OCT images of retinas injected with 7m8-rho-GFP (D), 7m8-rho-RS1 (E), or uninjected WT animals (F). Fundus images were taken through the inner nuclear layer of the superior retina and exclude other layers. (**G** to **I**) Transverse images of the superior (upper image) and inferior (lower image) retina were collected using the optic nerve head as a landmark. (**J**) Quantification of the mean full-field scotopic ERG b-wave amplitude resulting from a high-intensity (1 log cd × s/m^2) stimulus recorded on a monthly basis beginning 1 month after injection at P15. The increase in b-wave amplitude in 7m8-rho-RS1–treated eyes was significant at every time point (comparison to 1 month: $P = 0.006$, 2 months: $P = 0.019$, 3 months: $P < 0.0001$, and 4 months: $P < 0.0001$), whereas the response recorded from AAV2-rho-RS1–, AAV8-rho-RS1–, and 7m8-rho-RS1–injected eyes was the same as that from untreated *Rs1h*$^{-/-}$ eyes. $n = 7$ for all groups. Statistical analysis was a one-way analysis of variance (ANOVA) with post-hoc Tukey's multiple comparison performed with GraphPad Prism software. (**K**) Analysis of ERG responses under scotopic (upper traces, stimulus range from –3 to 1 log cd × s/m^2) and photopic (lower traces, range from –0.9 to 1.4 log cd × s/m^2) conditions. (**L**) Representative ERG traces from 7m8-rho-RS1–injected eyes show improved amplitude of the a- and b-wave and a waveform closer to WT eyes, compared to 7m8-rho-GFP–injected eyes.

significant restoration of the scotopic b-wave amplitude compared to the 7m8-CAG-GFP–treated contralateral control eye, or to AAV2-CAG-RPE65 (Fig. 5C; $P < 0.0001$, one-way ANOVA with post-hoc Tukey's multiple comparison). Representative ERG traces from 7m8-CAG-RPE65–and 7m8-CAG-GFP–injected eyes further illustrate this rescue of a- and b-wave amplitudes (Fig. 5D).

These results demonstrate that intravitreal 7m8-CAG-RPE65 administration yields substantial amounts of RPE65 protein expression in the RPE, resulting in considerable functional improvements in vision. Therefore, 7m8-mediated gene therapy can reach the deepest layers of a structurally intact retina and deliver therapeutic amounts of an important gene.

Intravitreal delivery of 7m8 transduces photoreceptors in the nonhuman primate retina

We further evaluated the clinical potential of our vector in nonhuman primates (male cynomolgus monkeys) in which the ILM is a significantly thicker physical barrier to the retina than in rodents (*19*, *20*, *33*) and thus poses greater challenges for intravitreal gene delivery. To date, only AAV2 has been intravitreally administered in macaques, leading to restricted transduction in a limited region around the macular RGCs (*34*–*37*). To assess the ability of 7m8 to extend gene delivery beyond the foveal region or deeper than the RGC layer, we intravitreally

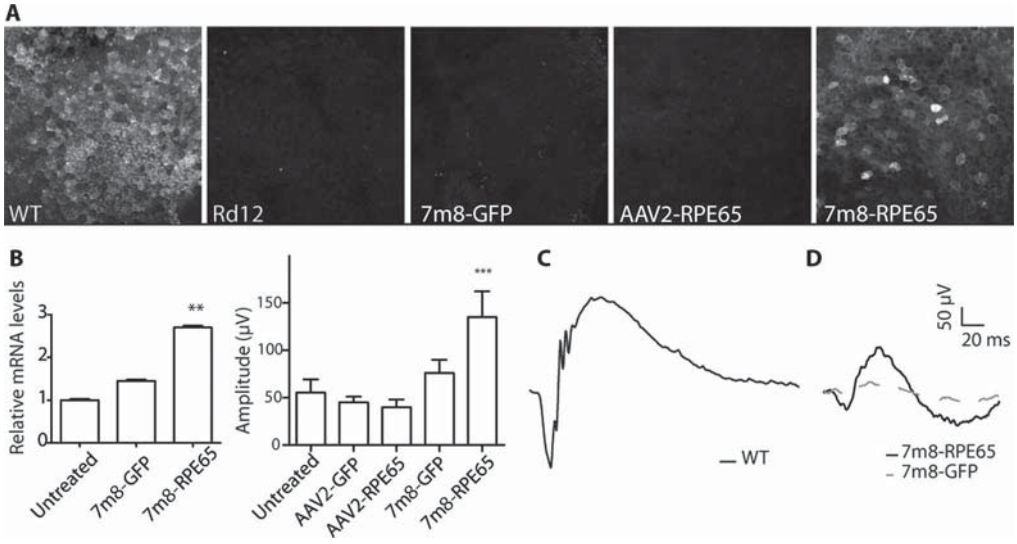

Fig. 5. Functional rescue in the *rd12* mouse retina after 7m8-mediated *RPE65* gene transfer. (**A**) Anti-RPE65 labeling. WT C57BL/6 mice expressed RPE65 across the RPE monolayer, whereas *rd12* mice lacked the RPE65 protein. Mice injected with 7m8-GFP and AAV2-RPE65 had no labeling of RPE65 protein. Mice injected with AAV2-RPE65 displayed low amounts of RPE65 in scattered RPE cells. In contrast, mice injected with 7m8-RPE65 displayed high levels of RPE65 expression in RPE cells. (**B**) RT-PCR from RNA extracted from RPE cells (which were dissected away from other retinal cells) revealed that levels of RPE65 mRNA were elevated in mice injected with 7m8-RPE65 but not in mice injected with 7m8-GFP or AAV2-RPE65. (**C**) ERG recordings revealed that the amplitude of the ERG b-wave was significantly increased ($P < 0.0001$) in mice injected with 7m8-RPE65 relative to other cohorts, whereas no significant differences were observed among ERGs recorded from mice injected with 7m8-GFP, AAV2-GFP, or the AAV2 vector expressing RPE65. (**D**) Representative ERG traces illustrate improved amplitude of the ERG in 7m8-scCAG-RPE65–injected (solid trace) compared to 7m8-GFP–injected eyes (dashed trace). $n = 7$ for all groups. Statistical analysis was a one-way ANOVA with post-hoc Tukey's multiple comparison performed with GraphPad Prism software.

administered 5×10^{12} viral particles of 7m8 with the cytomegalovirus (CMV) promoter driving expression of GFP (7m8-CMV-GFP) or the AAV2 quadruple tyrosine mutant (AAV2-4YF-CMV-GFP), again used as a comparison, in an adult macaque. GFP expression was subsequently assessed in vivo by funduscopic imaging.

In both cases, there was an initial moderate but self-resolving vitreal inflammation. At 3 weeks after injection, fluorescence imaging showed GFP expression for both vectors (Fig. 6, A and B). By 8 weeks, fluorescence levels increased for both vectors (Fig. 6, C and D); however, 7m8 mediated substantially higher gene expression both across the retina (Fig. 6, C and D) and inside the fovea (Fig. 6, G and H). At 12 weeks after injection, fundus imaging revealed signs of an immune response, likely a result of high levels of GFP, known to be an immunogenic protein (*38*, *39*). The study was halted, and histological analysis showed GFP expression in the extrafoveal photoreceptors in the 7m8-treated eye but not in the AAV2-4YF–treated eye (Fig. 6, E, F, and I to K, and fig. S8). We did not observe GFP expression in the RPE, in contrast to the results observed in mice, which showed high levels of transgene expression in this outermost layer. This may result from the fact that fewer viral particles were able to overcome the more substantial barriers in the primate retina, and, thus, fewer particles were able to reach the RPE adjacent to the transduced photoreceptors of the primate retina. The late-developing inflammation caused retinal thinning and damage in the highest GFP-expressing regions within the fovea, consistent with previous studies using high doses of AAV vectors that express GFP under the control of the CMV promoter in the nonhuman primate retina (*40*). Another macaque that received an injection of 5×10^{12} viral particles of 7m8 expressing GFP under the control of the neuronal promoter cx36 yielded a similar GFP expression pattern starting at 3 weeks after injection (fig. S9) but with no observable inflammation even after 16 weeks, further indicating that CMV promoter usage can yield a transgene-specific immune response against GFP. Regardless, these results indicate that 7m8 mediates strong amounts of transgene expression in the outer retina upon intravitreal administration to both rodents and nonhuman primates.

DISCUSSION

Our results illustrate the substantial potential of 7m8 for retinal gene therapy to treat diverse forms of inherited retinal degenerations affecting the inner and outer retina. More broadly, this work demonstrates that engineering AAV vector variants with properties designed to overcome critical biological transport and transduction barriers promises to make a wide range of diseases affecting complex tissues amenable to clinical gene therapy.

The landmark clinical trials for LCA2 gene therapy support the safety and efficacy of retinal gene transfer via AAV vectors (*5*–*8*) when the retinal structure is intact; however, the deteriorating retina in most degenerations make it challenging to build on the success of these clinical trials. We have demonstrated that AAV can be engineered to traverse several hundred micrometers of dense tissue—filled with extracellular matrix network, cell bodies, and processes—and dramatically increase gene delivery to important target cells far from a noninvasive injection site. This capability may substantially broaden the therapeutic potential for AAV to treat retinal neurodegeneration. Moreover, gene therapy approaches that require delivery across other complex tissue structures may also benefit from this engineering strategy, including endothelial barriers (for example, blood-brain, -retina, -muscle, or -tumor) upon systemic administration, or intraorgan or tumoral barriers upon local delivery. This approach, which selected viruses for the ability to penetrate the retina and infect a therapeutically relevant cell, advances on previous work that selected AAV libraries in vitro (*41*, *42*) or selected the virus in vivo for general localization to an organ after injection into the bloodstream (*43*, *44*).

The new AAV variant provided therapeutic amounts of transduction of photoreceptor cells and RPE after noninvasive administration to the vitreous humor of the eye in both normal murine retina and in models of human retinal disease. Furthermore, transduction

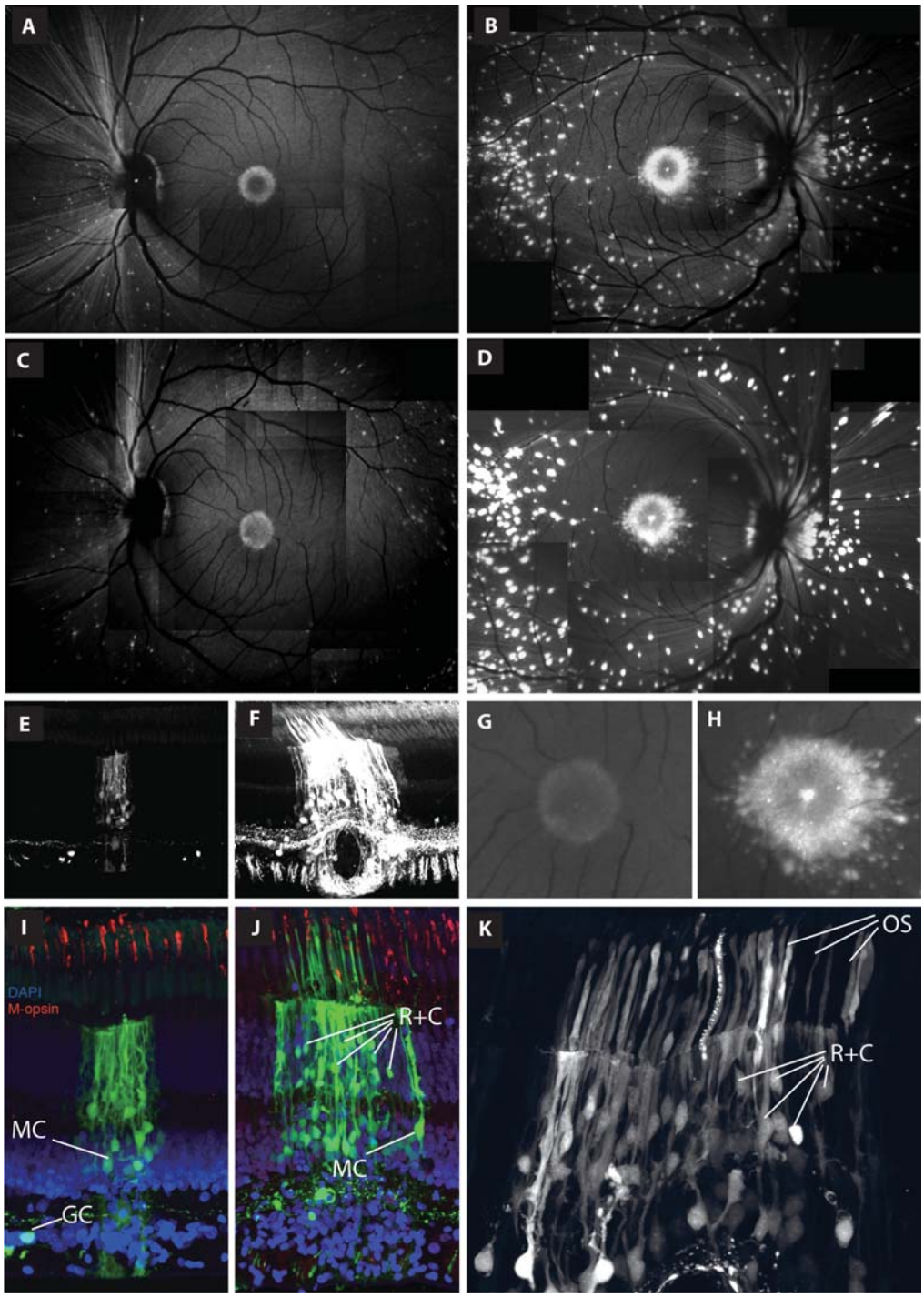

Fig. 6. AAV2-4YF– and 7m8-mediated GFP expression in primate retinas. (**A** to **D**) Fundus images of an adult macaque injected bilaterally with 5×10^{12} viral particles of either (A) AAV2-4YF-CMV-GFP or (B) 7m8-CMV-GFP 3 weeks after injection, and (C) AAV2-4YF-CMV-GFP and (D) 7m8-CMV-GFP at 8 weeks after injection. (**E** and **F**) Agarose sections through a brightly expressing fluorescent spot from peripheral retina in (E) AAV2-4YF-CMV-GFP– or (F) 7m8-CMV-GFP–injected eyes imaged at equal confocal acquisition settings. (**G** and **H**) Equal setting fundus imaging of the fovea in (G) AAV2-4YF-CMV-GFP– or (H) 7m8-CMV-GFP–injected retinas. (**I** and **J**) Confocal imaging through agarose sections of retinal sections injected with (I) AAV2-4YF-CMV-GFP or (J) 7m8-CMV-GFP imaged at adjusted settings for optimal detection of signal, costained with anti–m-opsin labeling in red. (**K**) High-magnification imaging of native GFP in macaque rods and cones resulting from injection of 7m8-CMV-GFP into the vitreous.

was strong in the nonhuman primate fovea—a region essential for high-acuity vision that may be damaged by detachment from the RPE during a subretinal injection (*12*)—as well as numerous regions beyond the fovea. Future engineering within nonhuman primates may enable even broader pan-retinal expression.

The creation of a new AAV variant that successfully transduces all retinal layers from the vitreous offers therapeutic potential for a broad array of additional inherited retinal degenerative diseases. The pan-retinal infective properties of 7m8, coupled with promoters or microRNA target regions to mediate cell-restrictive expression, make it a valuable vector for targeting other subsets of neurons in the retina. For example, 7m8 gene delivery of engineered light-sensitive channels, such as LiGluR (*45*) or other optogenetic tools including channelrhodopsin variants, to ON bipolar cells (*46*) or cone photoreceptor inner segments (*47*) may allow for the artificial restoration of light sensitivity in late stages of retinal degeneration.

The increased retinal transduction efficiency of 7m8 compared to its parental serotype AAV2 may arise from this variant's reduced heparin affinity, which may both decrease capsid sequestration in the ILM and enable enhanced penetration through retinal layers. Also, the peptide sequence could confer binding to a novel cell surface receptor or enhance intracellular viral trafficking. In any case, the high infectivity of the 7m8 capsid compared to previous vectors may enable the use of relatively low dosages, thereby reducing the chance of immune response to vector capsid protein, an important consideration for intravitreally delivered AAV vectors (*30*).

MATERIALS AND METHODS

Library generation and viral production

To generate the Y444F mutation on the AAV2 cap gene, as well as all subsequent tyrosine-to-phenylalanine mutations, we used a site-directed

mutagenesis kit (QuikChange Lightning, Agilent Technologies). As we have previously reported (*48*, *49*), random mutagenesis libraries were generated by subjecting the resulting AAV2 Y444F *cap* to error-prone PCR, as described. A 7mer peptide display library, created essentially as previously described (*24*), and an AAV library constructed by DNA shuffling of *cap* genes from AAV1, 2, 4, 5, 6, 8, and 9, as we have reported, (*26*) were also used. The rcAAV libraries and rAAV vectors expressing GFP under a CAG or Rho promoter were packaged as previously described (*26*, *48*), and deoxyribonuclease-resistant genomic titers were obtained through quantitative PCR.

Library selection and evolution

The libraries were pooled, and two rounds of evolution were performed, each consisting of initial library diversification followed by three in vivo selection steps. In each such step, P30 rho-GFP mice (*27*) were intravitreally injected with 2 ml of iodixanol-purified, phosphate-buffered saline (PBS)–dialyzed library with a genomic titer of about 1×10^{12} vg/ml. One week after injection, harvested retinas were dissociated with a light papain protease treatment, followed by FACS (Cytopeia Influx Cell Sorter, BD Biosciences) isolation of photoreceptor cells. DNA was extracted, and successful virions were PCR-amplified, recloned into the AAV genomic plasmid, and repackaged for the next injection. After three selection steps, the recovered *cap* genes were subjected to error-prone PCR, and then three additional selection steps. After this process, the *cap* genes of 48 variants were sequenced.

Molecular modeling

The amino acid residues were inserted into the Protein Data Bank (PDB) file 1LP3 (AAV2) at position 588 with Maestro software. This resultant data file was used in the Swiss Model homology mode with default, automated settings to build the VP3 monomer (Fig. 2B). The monomer was superposed onto the wild-type AAV2 VP3 monomer, and Viper (http://viperdb.scripps.edu/pdbToViper.php) was used to reconstruct the capsid.

Histological characterization of AAV transduction

P30 wild-type mice were used to analyze evolved variants. One to 3 months after intravitreal injection, retinas were extracted, and 10-μm-thick transverse cryosections were cut as described previously (*17*). Sections were analyzed by confocal microscopy (LSM5; Carl Zeiss). For immunohistochemistry on agarose embedded retinas, eyecups were embedded in 5% agarose and cut on a vibratome in a PBS bath. Sections were briefly postfixed, rinsed in PBS, and blocked before antibody labeling overnight at 4°C. Antibodies were the following: peanut agglutinin (PNA) (Molecular Probes, 1:200), anti–M-opsin (Chemicon International, 1:500), anti-RS1 (3R10 mouse monoclonal antibody, gift from R. Molday, 1:5), anti-synaptophysin (Abcam, 1:1000), anti-vimentin (Dako, 1:1000), anti-mGluR6 (Abcam, 1:1000), anti-IbaI (Abcam, 1:500), or anti-CD68 (Abcam, 1:500).

Electroretinograms

Electroretinograms were recorded (Espion E2 ERG System; Diagnosys LLC) in response to six light flash intensities ranging from −3 to 1 log cd × s/m^2 on a dark background as described previously (*17*). Each stimulus was presented in series of three. For photopic ERGs, the animal was first exposed to a rod-saturating background for 5 min. Stimuli ranging from −0.9 to 1.4 log cd × s/m^2 were presented 20 times on a lighted background. Data were analyzed with MATLAB (v7.7; MathWorks).

High-resolution SD-OCT

Images of retinal cross sections were averaged from eight contiguous slices. Histological imaging was performed with an 840-nm SDOIS (Spectral Domain Ophthalmic Imaging Systems) OCT system (Bioptigen). Retinal thickness, outer nuclear layer thickness, and photoreceptor inner and outer segment length measurements were gathered with InVivoVue software.

Primate retina

Intravitreal injections were made, with methods described previously (*34*), in one 11.2-kg male cynomolgus monkey that had tested negative for serum antibodies against AAV2. The right and left eyes were injected with 5×10^{12} viral particles of 7m8-CMV-GFP and AAV2- 4YF-CMV-GFP, respectively. Confocal scanning laser ophthalmoscopic images (Spectralis HRA, Heidelberg Engineering) were obtained from the two retinas at 3 and 8 weeks after injection, with autofluorescence settings, which leads to effective GFP visualization. At 12 weeks after injection, the monkey was euthanized, both retinas were lightly fixed in 4% paraformaldehyde, and tissue was examined via confocal microscopy. Pieces of primate retina were then embedded in 5% agarose and sectioned at 200 μm for immunocytochemistry.

Statistical analysis

Data were analyzed in GraphPad Prism version 5.00 (GraphPad Software) and are presented as means ± SD. As indicated in the results, data were compared with either a paired or an unpaired Student's *t* test or one-way ANOVA with post-hoc Tukey's multiple comparison. The difference was considered statistically significant if the *P* value was less than 0.05. In the figures, *P* values <0.05 are indicated by a single asterisk. *P* values <0.01 are indicated by a double asterisk. *P* values <0.001 are indicated by a triple asterisk. All analyses were two-tailed.

SUPPLEMENTARY MATERIALS

www.sciencetranslationalmedicine.org/cgi/content/full/5/189/189ra76/DC1

Fig. S1. Glycan dependencies of 7m8 compared to AAV2.
Fig. S2. GFP expression in photoreceptors after transduction with 7m8.
Fig. S3. GFP expression in the optic tract and brain histology after transduction with 7m8.
Fig. S4. Comparison of photoreceptor transduction by 7m8-rho-GFP and AAV2-4YF-rho-GFP.
Fig. S5. Immunolabeling for activated microglia and infiltrating macrophages after 7m8 readministration.
Fig. S6. Structural damage caused by subretinal injections in *Rs1h*$^{-/-}$ mice.
Fig. S7. Expression of control vectors and structural improvements at the photoreceptor–bipolar cell junction in *Rs1h*$^{-/-}$ mice.
Fig. S8. Expression of 7m8-CMV-GFP in nonhuman primate photoreceptor flat mounts.
Fig. S9. Expression of 7m8-cx36-GFP in nonhuman primate.
1LP3-mutant-swiss.pdb: PDB format data file for the modeling of the 7m8 capsid.

REFERENCES AND NOTES

1. T. Léveillard, J. A. Sahel, Rod-derived cone viability factor for treating blinding diseases: From clinic to redox signaling. *Sci. Transl. Med.* **2**, 26ps16 (2010).
2. E. M. Surace, A. Auricchio, Adeno-associated viral vectors for retinal gene transfer. *Prog. Retin. Eye Res.* **22**, 705–719 (2003).
3. C. Mussolino, M. della Corte, S. Rossi, F. Viola, U. Di Vicino, E. Marrocco, S. Neglia, M. Doria, F. Testa, R. Giovannoni, M. Crasta, M. Giunti, E. Villani, M. Lavitrano, M. L. Bacci, R. Ratiglia, F. Simonelli, A. Auricchio, E. M. Surace, AAV-mediated photoreceptor transduction of the pig cone-enriched retina. *Gene Ther.* **18**, 637–645 (2011).
4. S. G. Jacobson, T. S. Aleman, A. V. Cideciyan, A. Sumaroka, S. B. Schwartz, E. A. M. Windsor, E. I. Traboulsi, E. Heon, S. J. Pittler, A. H. Milam, A. M. Maguire, K. Palczewski, E. M. Stone, J. Bennett, Identifying photoreceptors in blind eyes caused by RPE65 mutations: Prerequisite for human gene therapy success. *Proc. Natl. Acad. Sci. U.S.A.* **102**, 6177–6182 (2005).

5. J. W. B. Bainbridge, A. J. Smith, S. S. Barker, S. Robbie, R. Henderson, K. Balaggan, A. Viswanathan, G. E. Holder, A. Stockman, N. Tyler, S. Petersen-Jones, S. S. Bhattacharya, A. J. Thrasher, F. W. Fitzke, B. J. Carter, G. S. Rubin, A. T. Moore, R. R. Ali, Effect of gene therapy on visual function in Leber's congenital amaurosis. *N. Engl. J. Med.* **358**, 2231–2239 (2008).
6. A. V. Cideciyan, T. S. Aleman, S. L. Boye, S. B. Schwartz, S. Kaushal, A. J. Roman, J. J. Pang, A. Sumaroka, E. A. M. Windsor, J. M. Wilson, T. R. Flotte, G. A. Fishman, E. Heon, E. M. Stone, B. J. Byrne, S. G. Jacobson, W. W. Hauswirth, Human gene therapy for RPE65 isomerase deficiency activates the retinoid cycle of vision but with slow rod kinetics. *Proc. Natl. Acad. Sci. U.S.A.* **105**, 15112–15117 (2008).
7. A. M. Maguire, K. A. High, A. Auricchio, J. F. Wright, E. A. Pierce, F. Testa, F. Mingozzi, J. L. Bennicelli, G. S. Ying, S. Rossi, A. Fulton, K. A. Marshall, S. Banfi, D. C. Chung, J. I. Morgan, B. Hauck, O. Zelenaia, X. Zhu, L. Raffini, F. Coppieters, E. De Baere, K. S. Shindler, N. J. Volpe, E. M. Surace, C. Acerra, A. Lyubarsky, T. M. Redmond, E. Stone, J. Sun, J. W. McDonnell, B. P. Leroy, F. Simonelli, J. Bennett, Age-dependent effects of RPE65 gene therapy for Leber's congenital amaurosis: A phase 1 dose-escalation trial. *Lancet* **374**, 1597–1605 (2009).
8. A. M. Maguire, F. Simonelli, E. A. Pierce, E. N. Pugh Jr., F. Mingozzi, J. Bennicelli, S. Banfi, K. A. Marshall, F. Testa, E. M. Surace, S. Rossi, A. Lyubarsky, V. R. Arruda, B. Konkle, E. Stone, J. Sun, J. Jacobs, L. Dell'Osso, R. Hertle, J. X. Ma, T. M. Redmond, X. Zhu, B. Hauck, O. Zelenaia, K. S. Shindler, M. G. Maguire, J. F. Wright, N. J. Volpe, J. W. McDonnell, A. Auricchio, K. A. High, J. Bennett, Safety and efficacy of gene transfer for Leber's congenital amaurosis. *N. Engl. J. Med.* **358**, 2240–2248 (2008).
9. A. F. Wright, C. F. Chakarova, M. M. A. El-Aziz, S. S. Bhattacharya, Photoreceptor degeneration: Genetic and mechanistic dissection of a complex trait. *Nat. Rev. Genet.* **11**, 273–284 (2010).
10. B. Lin, R. H. Masland, E. Strettoi, Remodeling of cone photoreceptor cells after rod degeneration in rd mice. *Exp. Eye Res.* **88**, 589–599 (2009).
11. T. M. Nork, C. J. Murphy, C. B. Y. Kim, J. N. Ver Hoeve, C. A. Rasmussen, P. E. Miller, H. D. Wabers, M. W. Neider, R. R. Dubielzig, R. J. McCulloh, B. J. Christian, Functional and anatomic consequences of subretinal dosing in the cynomolgus macaque. *Arch. Ophthalmol.* **130**, 65–75 (2012).
12. S. G. Jacobson, A. V. Cideciyan, R. Ratnakaram, E. Heon, S. B. Schwartz, A. J. Roman, M. C. Peden, T. S. Aleman, S. L. Boye, A. Sumaroka, T. J. Conlon, R. Calcedo, J. J. Pang, K. E. Erger, M. B. Olivares, C. L. Mullins, M. Swider, S. Kaushal, W. J. Feuer, A. Iannaccone, G. A. Fishman, E. M. Stone, B. J. Byrne, W. W. Hauswirth, Gene therapy for Leber congenital amaurosis caused by *RPE65* mutations: Safety and efficacy in 15 children and adults followed up to 3 years. *Arch. Ophthalmol.* **130**, 9–24 (2012).
13. L. L. Molday, W. W. H. Wu, R. S. Molday, Retinoschisin (RS1), the protein encoded by the X-linked retinoschisis gene, is anchored to the surface of retinal photoreceptor and bipolar cells through its interactions with a Na/K ATPase-SARM1 complex. *J. Biol. Chem.* **282**, 32792–32801 (2007).
14. S. Kjellstrom, R. A. Bush, Y. Zeng, Y. Takada, P. A. Sieving, Retinoschisin gene therapy and natural history in the *Rs1h*-KO mouse: Long-term rescue from retinal degeneration. *Invest. Ophthalmol. Vis. Sci.* **48**, 3837–3845 (2007).
15. A. Janssen, S. H. Min, L. L. Molday, N. Tanimoto, M. W. Seeliger, W. W. Hauswirth, R. S. Molday, B. H. Weber, Effect of late-stage therapy on disease progression in AAV-mediated rescue of photoreceptor cells in the retinoschisin-deficient mouse. *Mol. Ther.* **16**, 1010–1017 (2008).
16. S. H. Min, L. L. Molday, M. W. Seeliger, A. Dinculescu, A. M. Timmers, A. Janssen, F. Tonagel, N. Tanimoto, B. H. F. Weber, R. S. Molday, W. W. Hauswirth, Prolonged recovery of retinal structure/function after gene therapy in an *Rs1h*-deficient mouse model of X-linked juvenile retinoschisis. *Mol. Ther.* **12**, 644–651 (2005).
17. D. Dalkara, K. D. Kolstad, N. Caporale, M. Visel, R. R. Klimczak, D. V. Schaffer, J. G. Flannery, Inner limiting membrane barriers to AAV-mediated retinal transduction from the vitreous. *Mol. Ther.* **17**, 2096–2102 (2009).
18. M. Hellström, M. J. Ruitenberg, M. A. Pollett, E. M. E. Ehlert, J. Twisk, J. Verhaagen, A. R. Harvey, Cellular tropism and transduction properties of seven adeno-associated viral vector serotypes in adult retina after intravitreal injection. *Gene Ther.* **16**, 521–532 (2009).
19. M. D. Fischer, G. Huber, S. C. Beck, N. Tanimoto, R. Muehlfriedel, E. Fahl, C. Grimm, A. Wenzel, C. E. Remé, S. A. van de Pavert, J. Wijnholds, M. Pacal, R. Bremner, M. W. Seeliger, Noninvasive, in vivo assessment of mouse retinal structure using optical coherence tomography. *PLoS One* **4**, e7507 (2009).
20. D. M. Snodderly, R. S. Weinhaus, J. C. Choi, Neural–vascular relationships in central retina of macaque monkeys (*Macaca fascicularis*). *J. Neurosci.* **12**, 1169–1193 (1992).
21. H. Petrs-Silva, A. Dinculescu, Q. Li, S. H. Min, V. Chiodo, J. J. Pang, L. Zhong, S. Zolotukhin, A. Srivastava, A. S. Lewin, W. W. Hauswirth, High-efficiency transduction of the mouse retina by tyrosine-mutant AAV serotype vectors. *Mol. Ther.* **17**, 463–471 (2009).
22. H. Petrs-Silva, A. Dinculescu, Q. Li, W. T. Deng, J. J. Pang, S. H. Min, V. Chiodo, A. W. Neeley, L. Govindasamy, A. Bennett, M. Agbandje-McKenna, L. Zhong, B. Li, G. R. Jayandharan, A. Srivastava, A. S. Lewin, W. W. Hauswirth, Novel properties of tyrosine-mutant AAV2 vectors in the mouse retina. *Mol. Ther.* **19**, 293–301 (2011).
23. O. J. Müller, F. Kaul, M. D. Weitzman, R. Pasqualini, W. Arap, J. A. Kleinschmidt, M. Trepel, Random peptide libraries displayed on adeno-associated virus to select for targeted gene therapy vectors. *Nat. Biotechnol.* **21**, 1040–1046 (2003).
24. L. Perabo, H. Büning, D. M. Kofler, M. U. Ried, A. Girod, C. M. Wendtner, J. Enssle, M. Hallek, In vitro selection of viral vectors with modified tropism: The adeno-associated virus display. *Mol. Ther.* **8**, 151–157 (2003).
25. L. Zhong, B. Li, C. S. Mah, L. Govindasamy, M. Agbandje-McKenna, M. Cooper, R. W. Herzog, I. Zolotukhin, K. H. Warrington, K. A. Weigel-Van Aken, J. A. Hobbs, S. Zolotukhin, N. Muzyczka, A. Srivastava, Next generation of adeno-associated virus 2 vectors: Point mutations in tyrosines lead to high-efficiency transduction at lower doses. *Proc. Natl. Acad. Sci. U.S.A.* **105**, 7827–7832 (2008).
26. J. T. Koerber, J. H. Jang, D. V. Schaffer, DNA shuffling of adeno-associated virus yields functionally diverse viral progeny. *Mol. Ther.* **16**, 1703–1709 (2008).
27. F. Chan, A. Bradley, T. G. Wensel, J. H. Wilson, Knock-in human rhodopsin-GFP fusions as mouse models for human disease and targets for gene therapy. *Proc. Natl. Acad. Sci. U.S.A.* **101**, 9109–9114 (2004).
28. C. Summerford, R. J. Samulski, Membrane-associated heparan sulfate proteoglycan is a receptor for adeno-associated virus type 2 virions. *J. Virol.* **72**, 1438–1445 (1998).
29. W. Li, F. Kong, X. Li, X. Dai, X. Liu, Q. Zheng, R. Wu, X. Zhou, F. Lü, B. Chang, Q. Li, W. W. Hauswirth, J. Qu, J. J. Pang, Gene therapy following subretinal AAV5 vector delivery is not affected by a previous intravitreal AAV5 vector administration in the partner eye. *Mol. Vis.* **15**, 267–275 (2009).
30. Q. Li, R. Miller, P. Y. Han, J. Pang, A. Dinculescu, V. Chiodo, W. W. Hauswirth, Intraocular route of AAV2 vector administration defines humoral immune response and therapeutic potential. *Mol. Vis.* **14**, 1760–1769 (2008).
31. T. K. Park, Z. Wu, S. Kjellstrom, Y. Zeng, R. A. Bush, P. A. Sieving, P. Colosi, Intravitreal delivery of AAV8 retinoschisin results in cell type-specific gene expression and retinal rescue in the Rs1-KO mouse. *Gene Ther.* **16**, 916–926 (2009).
32. K. Bradshaw, N. George, A. Moore, D. Trump, Mutations of the XLRS1 gene cause abnormalities of photoreceptor as well as inner retinal responses of the ERG. *Doc. Ophthalmol.* **98**, 153–173 (1999).
33. S. Heegaard, O. A. Jensen, J. U. Prause, Structure of the vitread face of the monkey optic disc (*Macaca mulatta*). SEM on frozen resin-cracked optic nerveheads supplemented by TEM and immunohistochemistry. *Graefes Arch. Clin. Exp. Ophthalmol.* **226**, 377–383 (1988).
34. L. Yin, K. Greenberg, J. J. Hunter, D. Dalkara, K. D. Kolstad, B. D. Masella, R. Wolfe, M. Visel, D. Stone, R. T. Libby, D. Diloreto, D. Schaffer, J. Flannery, D. R. Williams, W. H. Merigan, Intravitreal injection of AAV2 transduces macaque inner retina. *Invest. Ophthalmol. Vis. Sci.* **52**, 2775–2783 (2011).
35. E. Ivanova, G. S. Hwang, Z. H. Pan, D. Troilo, Evaluation of AAV-mediated expression of Chop2-GFP in the marmoset retina. *Invest. Ophthalmol. Vis. Sci.* **51**, 5288–5296 (2010).
36. T. K. MacLachlan, M. Lukason, M. Collins, R. Munger, E. Isenberger, C. Rogers, S. Malatos, E. DuFresne, J. Morris, R. Calcedo, G. Veres, A. Scaria, L. Andrews, S. Wadsworth, Preclinical safety evaluation of AAV2-sFLT01—A gene therapy for age-related macular degeneration. *Mol. Ther.* **19**, 326–334 (2011).
37. C. Lebherz, A. M. Maguire, A. Auricchio, W. Tang, T. S. Aleman, Z. Wei, R. Grant, A. V. Cideciyan, S. G. Jacobson, J. M. Wilson, J. Bennett, Nonhuman primate models for diabetic ocular neovascularization using AAV2-mediated overexpression of vascular endothelial growth factor. *Diabetes* **54**, 1141–1149 (2005).
38. A. Gambotto, G. Dworacki, V. Cicinnati, T. Kenniston, J. Steitz, T. Tüting, P. D. Robbins, A. B. DeLeo, Immunogenicity of enhanced green fluorescent protein (EGFP) in BALB/c mice: Identification of an H2-K^d-restricted CTL epitope. *Gene Ther.* **7**, 2036–2040 (2000).
39. R. Stripecke, M. Carmen Villacres, D. Skelton, N. Satake, S. Halene, D. Kohn, Immune response to green fluorescent protein: Implications for gene therapy. *Gene Ther.* **6**, 1305–1312 (1999).
40. L. H. Vandenberghe, P. Bell, A. M. Maguire, C. N. Cearley, R. Xiao, R. Calcedo, L. Wang, M. J. Castle, A. C. Maguire, R. Grant, J. H. Wolfe, J. M. Wilson, J. Bennett, Dosage thresholds for AAV2 and AAV8 photoreceptor gene therapy in monkey. *Sci. Transl. Med.* **3**, 88ra54 (2011).
41. J. T. Koerber, R. Klimczak, J. H. Jang, D. Dalkara, J. G. Flannery, D. V. Schaffer, Molecular evolution of adeno-associated virus for enhanced glial gene delivery. *Mol. Ther.* **17**, 2088–2095 (2009).
42. R. R. Klimczak, J. T. Koerber, D. Dalkara, J. G. Flannery, D. V. Schaffer, A novel adeno-associated viral variant for efficient and selective intravitreal transduction of rat Müller cells. *PLoS One* **4**, e7467 (2009).
43. L. Yang, J. Jiang, L. M. Drouin, M. Agbandje-McKenna, C. Chen, C. Qiao, D. Pu, X. Hu, D. Z. Wang, J. Li, X. Xiao, A myocardium tropic adeno-associated virus, (AAV) evolved by DNA shuffling and in vivo selection. *Proc. Natl. Acad. Sci. U.S.A.* **106**, 3946–3951 (2009).
44. S. J. Gray, B. L. Blake, H. E. Criswell, S. C. Nicolson, R. J. Samulski, T. J. McCown, W. Li, Directed evolution of a novel adeno-associated virus (AAV) vector that crosses the seizure-compromised blood-brain barrier (BBB). *Mol. Ther.* **18**, 570–578 (2010).
45. N. Caporale, K. D. Kolstad, T. Lee, I. Tochitsky, D. Dalkara, D. Trauner, R. Kramer, Y. Dan, E. Y. Isacoff, J. G. Flannery, LiGluR restores visual responses in rodent models of inherited blindness. *Mol. Ther.* **19**, 1212–1219 (2011).
46. P. S. Lagali, D. Balya, G. B. Awatramani, T. A. Münch, D. S. Kim, V. Busskamp, C. L. Cepko, B. Roska, Light-activated channels targeted to ON bipolar cells restore visual function in retinal degeneration. *Nat. Neurosci.* **11**, 667–675 (2008).

47. V. Busskamp, J. Duebel, D. Balya, M. Fradot, T. J. Viney, S. Siegert, A. C. Groner, E. Cabuy, V. Forster, M. Seeliger, M. Biel, P. Humphries, M. Paques, S. Mohand-Said, D. Trono, K. Deisseroth, J. A. Sahel, S. Picaud, B. Roska, Genetic reactivation of cone photoreceptors restores visual responses in retinitis pigmentosa. *Science* **329**, 413–417 (2010).
48. N. Maheshri, J. T. Koerber, B. K. Kaspar, D. V. Schaffer, Directed evolution of adeno-associated virus yields enhanced gene delivery vectors. *Nat. Biotechnol.* **24**, 198–204 (2006).
49. J. T. Koerber, N. Maheshri, B. K. Kaspar, D. V. Schaffer, Construction of diverse adeno-associated viral libraries for directed evolution of enhanced gene delivery vehicles. *Nat. Protoc.* **1**, 701–706 (2006).

Acknowledgments: We thank K. Durkin of the Berkeley Molecular Graphics Facility for helping render visual representations of the 7m8 capsid; T. Lee for technical assistance with intraocular injections; A. Auricchio for sharing the AAV-rho-GFP plasmid; E. A. Zin for help with antibody labeling; and A. Visel and G. Niemeyer for the critical reading of the manuscript. B. Weber and B. Hauswirth provided the *Rs1h*$^{-/-}$ mice, and the rho-GFP mice were a gift from J. Wilson. We also thank R. Molday for the anti-RS1 antibody. **Funding:** This work was supported by grants from the NIH Nanomedicine Development Center for the Optical Control of Biological Function (PN2EY018241) and the Foundation Fighting Blindness USA. **Author contributions:** J.G.F., D.V.S., R.R.K., and D.D. conceived the in vivo–directed evolution strategy to screen for photoreceptor permissive AAVs. D.V.S. and J.G.F. supervised the project. D.D. and R.R.K. performed the directed evolution screen leading to 7m8 and its in vitro characterization. M.V. produced the recombinant AAVs. D.D. did the structural modeling of 7m8. L.C.B. and D.D. characterized in vivo transduction patterns of 7m8. L.C.B. designed and performed rescue experiments and did in vivo imaging as well as retinal and brain histology in mice. L.Y. and W.H.M. performed intraocular injections and realized live imaging in the nonhuman primates. L.C.B. performed histological analysis of nonhuman primate retinas. D.V.S., J.G.F., D.D., and L.C.B. designed the experiments, analyzed the data, and wrote the paper. **Competing interests:** D.D., J.G.F., and D.V.S. are inventors on pending patents related to AAV gene delivery.

Submitted 14 January 2013
Accepted 18 May 2013
Published 12 June 2013
10.1126/scitranslmed.3005708

Citation: D. Dalkara, L. C. Byrne, R. R. Klimczak, M. Visel, L. Yin, W. H. Merigan, J. G. Flannery, D. V. Schaffer, In vivo–directed evolution of a new adeno-associated virus for therapeutic outer retinal gene delivery from the vitreous. *Sci. Transl. Med.* **5**, 189ra76 (2013).